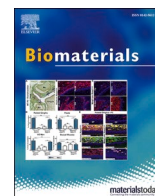




Since January 2020 Elsevier has created a COVID-19 resource centre with free information in English and Mandarin on the novel coronavirus COVID-19. The COVID-19 resource centre is hosted on Elsevier Connect, the company's public news and information website.

Elsevier hereby grants permission to make all its COVID-19-related research that is available on the COVID-19 resource centre - including this research content - immediately available in PubMed Central and other publicly funded repositories, such as the WHO COVID database with rights for unrestricted research re-use and analyses in any form or by any means with acknowledgement of the original source. These permissions are granted for free by Elsevier for as long as the COVID-19 resource centre remains active.



# AIEgen-loaded nanofibrous membrane as photodynamic/photothermal antimicrobial surface for sunlight-triggered bioprotection

Meng Li<sup>a,b</sup>, Haifei Wen<sup>a</sup>, Haoxuan Li<sup>a,b</sup>, Zhi-Chao Yan<sup>a,\*\*\*</sup>, Ying Li<sup>a</sup>, Lei Wang<sup>a</sup>, Dong Wang<sup>a,\*\*</sup>, Ben Zhong Tang<sup>c,d,\*</sup>

<sup>a</sup> Center for AIE Research, Shenzhen Key Laboratory of Polymer Science and Technology, Guangdong Research Center for Interfacial Engineering of Functional Materials, College of Materials Science and Engineering, Shenzhen University, Shenzhen, 518060, China

<sup>b</sup> Key Laboratory of Optoelectronic Devices and Systems of Ministry of Education and Guangdong Province, College of Physics and Optoelectronic Engineering, Shenzhen University, Shenzhen, 518060, China

<sup>c</sup> Department of Chemistry, Hong Kong Branch of Chinese National Engineering Research Center for Tissue Restoration and Reconstruction, The Hong Kong University of Science and Technology, Clear Water Bay, Kowloon, 999077, Hong Kong

<sup>d</sup> Shenzhen Institute of Aggregate Science and Technology, School of Science and Engineering, The Chinese University of Hong Kong, Shenzhen, Guangdong, 518172, China

## ARTICLE INFO

### Keywords:

Aggregation-induced emission  
Sunlight-triggered antimicrobial  
Personal protective equipment  
Electrospinning

## ABSTRACT

The outbreak of infectious diseases such as COVID-19 causes an urgent need for abundant personal protective equipment (PPE) which leads to a huge shortage of raw materials. Additionally, the inappropriate disposal and sterilization of PPE may result in a high risk of cross-contamination. Therefore, the exploration of antimicrobial materials possessing both microbe interception and self-decontamination effects to develop reusable and easy-to-sterilize PPE is of great importance. Herein, an aggregation-induced emission (AIE)-active luminogen-loaded nanofibrous membrane (TTVB@NM) sharing sunlight-triggered photodynamic/photothermal anti-pathogen functions are prepared using the electrospinning technique. Thanks to its porous nanostructure, TTVB@NM shows excellent interception effects toward ultrafine particles and pathogenic aerosols. Benefiting from the superior photophysical properties of the AIE-active dopants, TTVB@NM exhibits integrated properties of wide absorption in visible light range, efficient ROS generation, and moderate photothermal conversion performance. A series of antimicrobial evaluations reveal that TTVB@NM could effectively inactivate pathogenic aerosols containing bacteria (inhibition rate: >99%), fungi (~88%), and viruses (>99%) within only 10 min sunlight irradiation. This study represents a new strategy to construct reusable and easy-to-sterilize hybrid materials for potential bioprotective applications.

## 1. Introduction

In recent decades, emerging infectious diseases, such as H1N1 influenza, Middle East respiratory syndrome, Ebola, and COVID-19, have become a significant burden on the global economy and public health. Numerous experimental and clinical evidences demonstrated that personal protective equipment (PPE), like face masks, will help to prevent the spread of respiratory infections [1–3]. However, the outbreak of a pandemic usually causes a burst demand for such PPE, leading to a resource shortage worldwide. Additionally, the

inappropriate disposal and sterilization of PPE may cause a high risk of cross-contamination and further disease spreading because the pathogens intercepted on the PPE are still highly infectious [4]. Therefore, there is an urgent need for antimicrobial materials possessing both microbe interception and decontamination effects to develop reusable and easy-to-sterilize PPE [5]. To that end, one simple yet appealing strategy is to fabricate hybrid thin-film materials by incorporating biocidal agents through either physical doping or chemical conjugation. The promising biocidal agents currently used as dopants include quaternary ammonium compounds, *N*-halamines, antimicrobial peptides,

\* Corresponding author. Department of Chemistry, Hong Kong Branch of Chinese National Engineering Research Center for Tissue Restoration and Reconstruction, The Hong Kong University of Science and Technology, Clear Water Bay, Kowloon, 999077, Hong Kong.

\*\* Corresponding author.

\*\*\* Corresponding author.

E-mail addresses: [wangd@szu.edu.cn](mailto:wangd@szu.edu.cn) (D. Wang), [tangbenz@ust.hk](mailto:tangbenz@ust.hk) (B.Z. Tang).

<https://doi.org/10.1016/j.biomaterials.2021.121007>

Received 24 March 2021; Received in revised form 30 June 2021; Accepted 1 July 2021

Available online 3 July 2021

0142-9612/© 2021 Elsevier Ltd. All rights reserved.

nanoparticles of noble metals and metal oxides [6–8]. However, they usually suffer from a long treatment time for efficient decontamination or lack a broad-spectrum inactivation effect against various microbes including bacteria, fungi, and viruses [9,10].

Photosensitizers (PSs) have recently emerged as promising candidates for antimicrobial applications benefiting from the facile remote-control using light and negligible drug resistance [11–16]. The toxic reactive oxygen species (ROS) generated by PSs upon light exposure could rapidly react with broad-spectrum microbes (including both Gram-positive and -negative bacteria, fungi, and viruses with capsid and lipid envelopes), significantly reducing the risk of further infections. ROS mainly include singlet oxygen ( $^1\text{O}_2$ ), superoxide anion radical ( $\text{O}_2^-$ ), and hydroxyl radical ( $\bullet\text{OH}$ ). The diffusion distance of  $^1\text{O}_2$  in air (2–3.5 mm) is much longer than in water (300 nm), endowing the capability of PSs-immobilized coatings and textiles to remotely inactivate bacteria and viruses in air via  $^1\text{O}_2$  [17–20].  $\text{O}_2^-$  (few seconds) has a much longer half-life than  $^1\text{O}_2$  ( $10^{-5}$  s) and hydroxyl radical  $\bullet\text{OH}$  ( $10^{-9}$  s) [21–23], therefore,  $\text{O}_2^-$  appears to have a relatively long diffusion distance among others. In addition,  $\text{O}_2^-$  could be further converted to  $\bullet\text{OH}$  radicals which are considered as the most powerful oxidizing species for microbial inactivation and pollution degradation [24,25]. To date, most PSs that could generate  $\text{O}_2^-$  and  $\bullet\text{OH}$  are inorganic semiconducting materials such as  $\text{TiO}_2$ ,  $\text{ZnO}$ , and  $\text{SnWO}_4$  and they usually require UV or blue light for excitation [26,27]. Compared with the inorganic materials, organic PSs exhibit a few advantages including simple processing into flexible hybrid materials via either physical doping or chemically conjugation, tunable energy bandgap, and structure diversity. Thus, the development of organic PSs capable of producing  $\text{O}_2^-$  and highly toxic  $\bullet\text{OH}$  as antimicrobial agents has recently aroused a lot of interest. Among all the organic PSs that have been reported, PSs with aggregation-induced emission (AIE) characteristics have attracted increasing attention since some AIE-active PSs were demonstrated to exhibit a unique aggregation-induced enhancement of ROS [28,29]. So far, AIE-active PSs have been successfully developed for microbe detection, discrimination, and infection treatment [30–34]. Other than that, by precise molecular design in terms of adjusting the  $\pi$ -conjugation system and engineering the electron donor-acceptor moiety, AIE luminogens (AIEgens) with wide color tunability in the visible light range could be obtained, allowing for a white light-driven biocidal effect [35,36]. In addition, the existence of molecular rotors

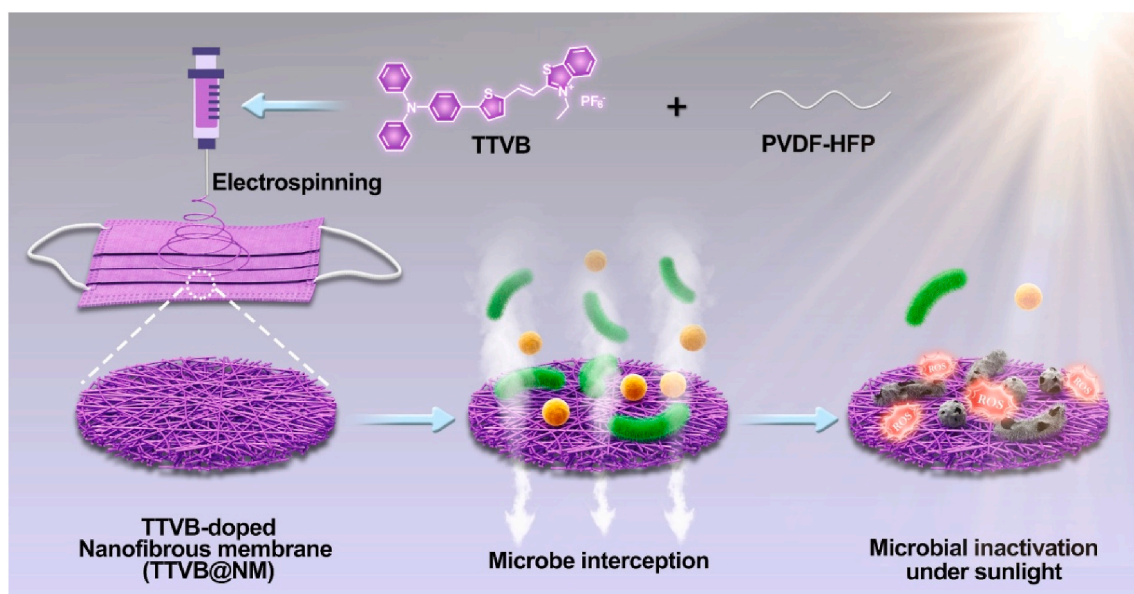
in the AIEgen skeleton could facilitate excited-state energy dissipation via non-radiative decay and thus promote photothermal conversion [37, 38]. Combining these unique features, a few AIEgens were developed for synergistic photodynamic and photothermal treatment by making full use of both ROS and heat [39–41]. However, those researches mostly focused on the bacteria killing in solution or infection treatment in vivo, researches regarding the fabrication of AIEgen-loaded hybrid material as antimicrobial surfaces are still rare.

In this work, a new nanofibrous membrane, namely TTVB@NM, comprising of AIEgen TTVB as the dopant and an electroactive polymer PVDF-HFP as the matrix is fabricated by the electrospinning technique (Scheme 1). The multi-layered porous structure of TTVB@NM favors the interception of pathogenic droplets and aerosols. Upon sunlight irradiation, TTVB@NM is capable of generating massive ROS, which plays a dominant role for the microbicidal effect, and exhibiting a moderate photothermal conversion performance which plays an adjuvant role for the microbe inhibition, synergistically endowing its effective application for sunlight-triggered inactivation of various microbes including bacteria, fungi, and viruses.

## 2. Experimental section

### 2.1. Materials and instruments

Luria-Bertani (LB) broth (L1010), Yeast Peptone Dextrose (YPD) broth (LA5010), and agar powder (A8190) were provided by Beijing Solarbio Science & Technology Co., Ltd. Isopropyl  $\beta$ -D-thiogalactopyranoside (IPTG, A600168), 5-bromo-4-chloro-3-indolyl- $\beta$ -D-galactopyranoside (X-gal, A600083), and tetracycline hydrochloride (A100422) were purchased from Shanghai Sangon Biotech Co., Ltd. Poly(vinylidene fluoride-co-hexafluoropropylene) (PVDF-HFP) (average Mw  $\sim$  400 k) was obtained from Sigma-Aldrich. Other chemicals and reagents were purchased from Shanghai Aladdin Biochemical Technology Co., Ltd. or J&K Scientific Ltd. and they were used as purchased without further purification. All the NMR spectra were recorded on a Bruker AVANCE III 500 MHz and 600 MHz (Bruker, Germany). Morphology of nanofibrous membrane was observed on a Thermo scientific APREO S high-resolution scanning electron microscope (SEM). Confocal laser scanning microscope (CLSM) images were taken on a Zeiss LSM880 (Carl Zeiss AG, Germany). UV-vis absorption spectra were



**Scheme 1.** Schematic illustration of the preparation of TTVB-loaded nanofibrous membrane (TTVB@NM) through electrospinning for microbe interception and microbial inactivation under sunlight.

recorded on a PerkinElmer Lambda 950 (PerkinElmer, USA). Fluorescence emission spectra were recorded on an FS 5 fluorescence spectrometer (Edinburgh Instruments, UK). White light source (400–800 nm) with a xenon lamp (CXE-350) was provided by OPT photoelectric technology LTD (Beijing, China). The water contact angle was measured using a DSA100S drop shape analyzer (Kruss, Germany) by dropping 2  $\mu\text{L}$  of distilled water on the membrane. Photothermal conversion performance was monitored by an E6 IR-camera (FLIR, USA). Pathogen aerosols were prepared by an aerosol generator Yuwell 403 E (Yuwell Medical Equipment Co., LTD, China). According to the ASTM D737 criterion, the air permeability of the nanofibrous membranes was evaluated using an automatic permeability instrument (YG 461 E) (Ningbo Textile Instruments, China) with a differential pressure of 200 Pa and the testing area of the nanofibrous membrane was 20  $\text{cm}^2$ . The filtration efficiency and pressure drop were tested on an Automated Filter Tester Model TSI 8130 (TSI Incorporated, USA) with a testing area of 100  $\text{cm}^2$ .

## 2.2. Synthesis of TTVB

5-[4-(Diphenylamino)phenyl]thiophene-2-carbaldehyde (780 mg, 2.2 mmol) and 3-ethyl-2-methylbenzo [d]thiazol-3-ium iodide (0.61 g, 2.0 mmol) were dissolved in anhydrous ethanol (100 mL) and a few drops of piperidine (catalytic amount), and then refluxed under the nitrogen atmosphere for 24 h. After cooling down to room temperature, the mixture was concentrated under vacuum and further purified by silica-gel chromatography (dichloromethane/methanol as eluent) to yield an intermediate product. Then the intermediate product (0.66 g, 1.0 mmol) was dissolved in acetone (20 mL) and mixed with saturated potassium hexafluorophosphate aqueous solution (20 mL). The mixture was refluxed for 2 h and filtered to yield a magenta precipitate. The precipitates were washed with water and then dried in the vacuum to obtain the final product (yield 80%).  $^1\text{H}$  NMR (500 MHz,  $\text{DMSO-}d_6$ ,  $\delta$ ): 8.45 (d,  $J = 15.3$  Hz, 1H), 8.40 (dd,  $J = 8.1, 1.1$  Hz, 1H), 8.25 (d,  $J = 8.4$  Hz, 1H), 7.97 (d,  $J = 4.0$  Hz, 1H), 7.85 (ddd,  $J = 8.5, 7.2, 1.3$  Hz, 1H), 7.79–7.74 (m, 1H), 7.69 (d,  $J = 8.7$  Hz, 2H), 7.66 (d,  $J = 4.0$  Hz, 1H), 7.63 (d,  $J = 15.4$  Hz, 1H), 7.38 (dd,  $J = 8.4, 7.4$  Hz, 4H), 7.15 (t,  $J = 7.4$  Hz, 2H), 7.13–7.08 (m, 4H), 6.99 (d,  $J = 8.8$  Hz, 2H), 4.90 (q,  $J = 7.2$  Hz, 2H), 1.45 (t,  $J = 7.2$  Hz, 3H).  $^{19}\text{F}$  NMR (500 MHz,  $\text{DMSO-}d_6$ ,  $\delta$ ): 69.40, 70.91.  $^{13}\text{C}$  NMR (151 MHz,  $\text{DMSO-}d_6$ ,  $\delta$ ): 170.60, 151.92, 148.52, 146.35, 141.54, 140.89, 137.78, 137.20, 129.82, 129.40, 128.12, 127.98, 127.16, 125.58, 125.10, 124.84, 124.34, 124.24, 121.61, 116.32, 109.96, 44.15, 40.06, 14.10. HRMS (ESI)  $m/z$ :  $[\text{M} - \text{PF}_6]^+$  calcd for  $\text{C}_{33}\text{H}_{27}\text{N}_2\text{S}_2$ , 515.1610; found, 515.1596.

## 2.3. ROS generation measurement of TTVB

(1) DCFH as an indicator for total ROS: The commercially available DCFH-DA was firstly converted to DCFH by mixing 100  $\mu\text{L}$  of DCFH-DA stocking solution (1 mM) in ethanol with 400  $\mu\text{L}$  of 0.01 M NaOH aqueous solution and allowed to sit at room temperature for 30 min. The above solution was neutralized with 19.5 mL of PBS solution at pH 7.4 to make a final concentration of 5  $\mu\text{M}$ . Then, TTVB or RB stocking solution in DMSO (1 mM) was added to make a final concentration of photosensitizer at 2  $\mu\text{M}$ . The fluorescence emission intensities of the mixed solution at 525 nm (Ex: 485 nm) were recorded before and after irradiation with a xenon lamp ( $34 \text{ mW cm}^{-2}$ ) for different time intervals. (2) ABDA as an indicator for  $^1\text{O}_2$ : ABDA was dissolved in DMSO to make a stocking solution of 25 mM. In a typical test, ABDA was diluted to 50  $\mu\text{M}$  with distilled water and then TTVB or RB stocking solution in DMSO (1 mM) was added to make a final concentration of photosensitizer at 5  $\mu\text{M}$ . The absorption spectra of the mixed solution at 350–420 nm were recorded before and after irradiation with a xenon lamp ( $34 \text{ mW cm}^{-2}$ ) for different time intervals. (3) DHR 123 as an indicator for  $\text{O}_2^-$ : DHR 123 was dissolved in DMSO to make a stocking solution of 10 mM. In a typical test, DHR 123 was diluted to 10  $\mu\text{M}$  with PBS and then TTVB or RB stocking solution in DMSO (1 mM) was added to make a final

concentration of photosensitizer at 2  $\mu\text{M}$ . The fluorescence emission intensities of the mixed solution at 535 nm (Ex: 505 nm) were recorded before and after irradiation with a xenon lamp ( $34 \text{ mW cm}^{-2}$ ) for different time intervals. (4) HPF as indicator for  $\bullet\text{OH}$ : HPF was dissolved in DMF to make a stocking solution of 5 mM. In a typical test, HPF was diluted to 5  $\mu\text{M}$  with PBS and then TTVB or RB stocking solution in DMF was added to make a final concentration of photosensitizer at 2  $\mu\text{M}$ . The fluorescence emission intensities of the mixed solution at 515 nm (Ex: 495 nm) were recorded before and after irradiation with a xenon lamp ( $34 \text{ mW cm}^{-2}$ ) for different time intervals.

## 2.4. Microbes preparation

*S. aureus* and multidrug-resistant *S. aureus* (MRSA) were chosen as the model Gram-positive bacteria. *E. coli* and multi-drug resistant *E. coli* (MDR *E. coli*) were chosen as the model Gram-negative bacteria. All the four strains were cultured in LB broth or on LB broth agar plate. *C. albicans* and *S. cerevisiae* were chosen as the model fungi and were cultured in YPD broth or on YPD broth agar plate. M13 bacteriophage was chosen as the model virus and *E. coli* strain (ER2738, New England Biolabs Inc., catalog #E4104) was used as the host. ER2738 was cultured in LB broth containing 20  $\mu\text{g/mL}$  tetracycline.

A single colony of bacteria or fungi was transferred into LB or YPD broth for overnight culture at 37  $^\circ\text{C}$  with a shaking speed of 200 rpm. We then inoculate a 5 mL culture in a 15 mL sterile Falcon tube with 5  $\mu\text{L}$  overnight culture to mid-log phase. Cultures were centrifuged at 7000 rpm for 2 min and pellets collected were washed two times with PBS and finally dispersed in PBS for further use.

In the case of M13 bacteriophage, M13 pellets were collected by a typical PEG-NaCl precipitation method, diluted in Tris-NaCl buffer (TBS), and quantified on LB/IPTG/X-gal plates. M13 was diluted in TBS buffer to  $10^{12}$  plaque-forming units per milliliter ( $\text{pfu mL}^{-1}$ ) and stocked at 4  $^\circ\text{C}$  for further use.

## 2.5. CLSM imaging of different microbes with TTVB

Freshly prepared bacterial or fungal suspension in PBS was diluted to an  $\text{OD}_{600}$  of 1.0 and treated with different amounts of TTVB at a certain concentration (2  $\mu\text{M}$  for Gram-positive bacteria and fungi, 10  $\mu\text{M}$  for Gram-negative bacteria). After incubation at 37  $^\circ\text{C}$  for 20 min, the bacteria or fungi were harvested by centrifugation and then resuspended in PBS. For the colocalization experiments with other trackers, the bacteria or fungi treated with TTVB were washed with PBS twice and then stained with 5  $\mu\text{g/mL}$  Hoechst 33,342 or 1  $\mu\text{M}$  Mito-tracker in PBS for 20 min. Before taking confocal images, 2  $\mu\text{L}$  of stained bacteria solution was transferred to a glass slide and then covered by a coverslip.

## 2.6. Antimicrobial tests of TTVB against different microbes

Freshly prepared bacteria or fungi suspension in PBS was diluted to an  $\text{OD}_{600}$  of 0.01. M13 suspension in TBS was diluted to  $10^8$   $\text{pfu mL}^{-1}$ . To the microbe suspensions, was added TTVB solution to a defined final concentration (500 nM for M13, 1  $\mu\text{M}$  for Gram-positive bacteria and fungi, 5  $\mu\text{M}$  for Gram-negative bacteria). The mixture was then incubated at 37  $^\circ\text{C}$  for 20 min and then irradiated under the simulated sunlight for 10 min at an optical intensity of  $34 \text{ mW cm}^{-2}$ , while the control groups were kept in the dark for 10 min. The pathogen suspensions were serially diluted to be planted on LB-agar plates (100  $\mu\text{L}$  of bacteria solution for each plate), YPD-agar plates (100  $\mu\text{L}$  of fungi solution for each plate), or LB/IPTG/X-gal plates (10  $\mu\text{L}$  M13 phage solution in TBS + 200  $\mu\text{L}$  ER2738 in TBS + 3 mL Top-agar solution for each plate) which was then subjected to incubation at 37  $^\circ\text{C}$  before quantification and being taken photos.

## 2.7. Preparation of nanofibrous membrane (TTVB@NM)

The solution for electrospinning was prepared by dissolving 1.8 g of PVDF-HFP and 90 mg of TTVB in a 10 mL mixture of THF and DMF (v/v = 7:3). The solution was stirred at 45 °C overnight for fully dissolving and then loaded into a 5-mL plastic syringe capped with a 21-gauge needle. A programmable syringe pump (KD Scientific) was used to eject the solution with a flow rate of 1 mL per hour. The voltage was maintained at 13.5 kV generated by Gamma High Voltage. The distance between the tip of the needle and the collecting aluminum foil was 15 cm. For all the antimicrobial tests, TTVB@NM was prepared with an electrospinning time of 30 min. The resulting TTVB@NM was further dried in a vacuum at 45 °C overnight to remove any residual solvent and then stocked in dark. For the tests of filtration efficiency, pressure drop, and air-permeability, TTVB@NM was collected on a piece of commercially provided melt-blowing fabric (MBF, thickness: 150 μm) as support.

## 2.8. ROS generation measurement of TTVB@NM

NM or TTVB@NM were cut to  $0.3 \times 0.3 \text{ cm}^2$  and attached to the bottom of a 24-well plate. Then, 600 μL of DCFH or HPF solution (5 μM) in PBS was added to each well. The fluorescence emission intensities in each well at 525 nm (Ex: 485 nm) were recorded before and after irradiation with a xenon lamp ( $34 \text{ mW cm}^{-2}$ ) for different time intervals.

## 2.9. Antimicrobial tests of TTVB@NM against different microbes in aqueous droplets

Freshly prepared bacteria and fungi suspensions in PBS were diluted to an  $\text{OD}_{600}$  of 0.1. M13 suspension in TBS was diluted to  $10^{10} \text{ pfu mL}^{-1}$ . In a typical experiment, 10 μL of microbe suspension was spotted on the surface of NM or TTVB@NM samples ( $0.5 \text{ cm} \times 0.5 \text{ cm}$ ). Then the samples were exposed to simulated sunlight ( $65 \text{ mW cm}^{-2}$ ) or dark conditions for a certain time interval. After that, the microbes on the surface of NM or TTVB@NM were collected by washing the samples with 1 mL of PBS buffer and then serially diluted to be planted on LB-agar, YPD-agar, or LB/IPTG/X-gal plates, which was then subjected to incubation at 37 °C before quantification and being taken photos.

For the SEM sampling, the collected bacteria or fungi pellets were firstly fixed in PBS solution containing 2.5% glutaraldehyde at 4 °C overnight and then rinsed with water, followed by dehydration with a sequential ethanol/water mixtures with an increasing ethanol volume of 30%, 50%, 70%, 80%, 90%, 95%, and 100%, respectively. Finally, the samples were dropped on a silicon wafer, vacuum dried, and coated with palladium before SEM analysis.

## 2.10. Antimicrobial tests of TTVB@NM against pathogenic aerosols

Freshly prepared bacteria (*E. coli* and *S. aureus*) suspensions in PBS were diluted to an  $\text{OD}_{600}$  of 0.01 in 10 mL of PBS and then loaded into the aerosol generator. The bacterial aerosols were sprayed to the surface of NM or TTVB@NM ( $1.5 \text{ cm} \times 1.5 \text{ cm}$ ) at a distance of 2 cm for 20 s. Immediately after that, the NM or TTVB@NM in 35 mm Petri dishes were transferred under the xenon lamp ( $65 \text{ mW cm}^{-2}$ ) to irradiate or kept in dark for 5 or 10 min. Subsequently, NM and TTVB@NM were washed thoroughly with 1 mL of PBS to be planted on LB plates, which were then subjected to incubation at 37 °C before quantification and being taken photos. Similar processes were also performed with fungi (*C. albicans*) and M13 bacteriophage, whereas the concentration of *C. albicans* in PBS is 1.0  $\text{OD}_{600}$ , and that of M13 bacteriophage in TBS is  $10^{10} \text{ pfu per milliliter}$ .

## 2.11. Antimicrobial tests of TTVB@NM against mixing microbes in aerosols under natural sunlight

Four different pathogens (*E. coli*, *S. aureus*, *C. albicans*, and M13 bacteriophage) were mixed in 10 mL of PBS buffer. The final concentration of both *E. coli* and *S. aureus* is around 0.01  $\text{OD}_{600}$ . The final concentration of *C. albicans* is around 1.0  $\text{OD}_{600}$ . The final concentration of M13 is around  $10^{10} \text{ pfu mL}^{-1}$ . The suspension mixture was then loaded into the aerosol generator. The pathogenic aerosols were sprayed to the surface of NM or TTVB@NM at a distance of 2 cm for 20 s. Immediately after that, the NM or TTVB@NM ( $1.5 \text{ cm} \times 1.5 \text{ cm}$ ) in 35 mm Petri dishes were transferred under the natural sunlight (outdoor temperature: 26 °C, the optical intensity of sunlight:  $83 \text{ mW cm}^{-2}$ ) to irradiate or kept in dark for 5 or 10 min. Subsequently, NM and TTVB@NM were washed thoroughly with 1 mL of PBS to be planted on LB plates, which were then subjected to incubation at 37 °C before quantification and being taken photos.

## 3. Results and discussion

### 3.1. Synthesis of TTVB

TTVB was facilely synthesized on a large scale from the condensation between 5-[4-(diphenylamino)phenyl]thiophene-2-carbaldehyde and 3-ethyl-2-methylbenzo [d]thiazolium iodide followed by a counterion exchanging reaction. The structure of TTVB was characterized using proton nuclear magnetic resonance ( $^1\text{H NMR}$ ),  $^{19}\text{F NMR}$ ,  $^{13}\text{C NMR}$ , and high-resolution mass (HRMS) (Fig. S1~S3). The fluorescence quantum yields (QYs) of TTVB in a well-dissolved state in dimethylsulfoxide (DMSO) and aggregated state in DMSO/toluene (v/v = 1:19) were determined to be 0.6% and 5.3%, respectively, indicating the AIE characteristic of TTVB.

TTVB possesses a typical donor- $\pi$ -acceptor (D- $\pi$ -A) structure comprising of triphenylamine fragment acting as an electron-donating unit, vinylthiophene group as a  $\pi$  bridge, and 3-ethylbenzo [d]thiazol-3-ium group as an electron-accepting moiety. PSs with D-A structure and heteroatoms (such as S and N) were demonstrated to have promoted ROS generation efficiency resulting from the sufficient intersystem crossing (ISC) process [42,43]. TTVB solid has a broad absorption in the white light range (400–700 nm) with an absorption maximum at 552 nm which will benefit the sunlight-triggered ROS generation (Fig. S4).

### 3.2. Evaluation of ROS generation efficiency of TTVB

ROS generation efficiency of TTVB was evaluated using different indicators under the irradiation of a white light source to simulate the sunlight (Fig. 1A–D). The commercial photosensitizer Rose Bengal (RB), which is known to have a high ROS generation efficiency, was utilized as a reference material. 2',7'-Dichlorodihydrofluorescein (DCFH) is a commonly used indicator to sense the amount of total ROS generation [44]. The non-fluorescent DCFH could be oxidized to strong fluorescent DCF ( $\lambda_{\text{ex}}$ : 485 nm,  $\lambda_{\text{em}}$ : 525 nm) by ROS. As illustrated in Fig. 1A, TTVB definitely outperforms RB in terms of ROS production under simulated sunlight irradiation ( $34 \text{ mW cm}^{-2}$ ). ROS type generated by TTVB was next distinguished using 9,10-anthracenediyl-bis(methylene) dimalonate (ABDA), dihydrorhodamine 123 (DHR 123), and hydroxyphenyl fluorescein (HPF) as indicators for detecting  $^1\text{O}_2$ ,  $\text{O}_2^{\bullet -}$ , and  $\bullet\text{OH}$ , respectively (Fig. 1B–D). It was revealed that TTVB generated less  $^1\text{O}_2$  but more  $\text{O}_2^{\bullet -}$  and  $\bullet\text{OH}$  than RB under simulated sunlight irradiation.  $\text{O}_2^{\bullet -}$  exhibits a much longer half-life time than  $^1\text{O}_2$ , benefiting its diffusion in a long distance.  $\text{O}_2^{\bullet -}$  could be further transformed to highly toxic  $\bullet\text{OH}$ , which is favorable for the efficient inactivation of pathogenic microbes. In addition, TTVB has a moderate photochemical conversion performance under simulated sunlight (Fig. S5), which is expected to assist the pathogen killing without causing discomfort while in contact with the mouth and skin. Given the broad absorption in the white light

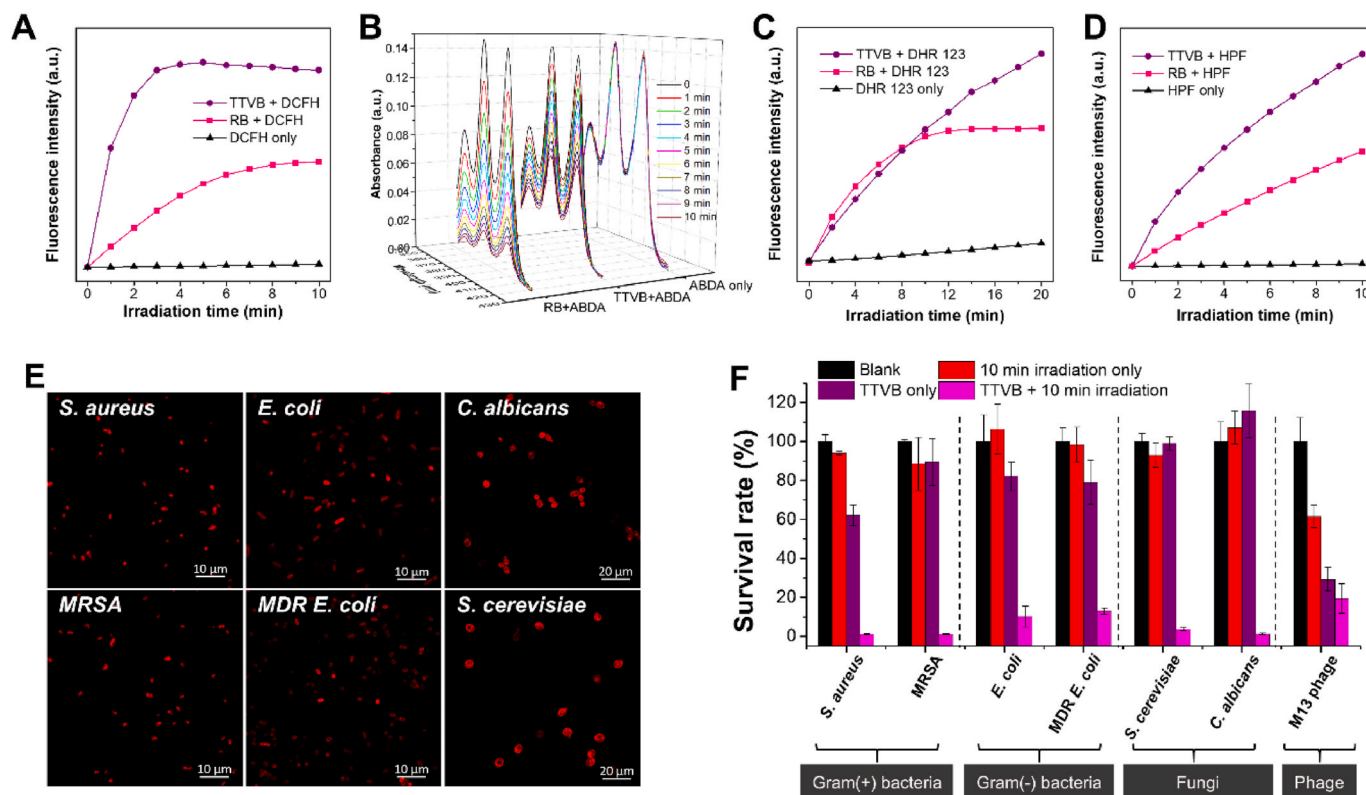


**Fig. 1.** (A–D) ROS generation ability of TTVB in aqueous solution upon light irradiation ( $34 \text{ mW cm}^{-2}$ ) verified with different ROS indicators: (A) DCFH as the indicator for total ROS; (B) ABDA as the indicator for  $^1\text{O}_2$ ; (C) DHR 123 as the indicator for  $\text{O}_2^-$ ; (D) HPF as the indicator for  $\bullet\text{OH}$ . (E) CLSM images of different bacteria and fungi stained with TTVB ( $10 \mu\text{M}$  for *E. coli* and MDR *E. coli*;  $2 \mu\text{M}$  for *S. aureus*, MDR *S. aureus*, *S. cerevisiae*, and *C. albicans*). (F) Antimicrobial activity of TTVB ( $5 \mu\text{M}$  for Gram-negative bacteria;  $1 \mu\text{M}$  for Gram-positive bacteria and fungi;  $500 \text{ nM}$  for M13 phage) upon irradiation with simulated sunlight ( $34 \text{ mW cm}^{-2}$ ).

range, the high ROS generation efficiency, and moderate photothermal conversion performance of TTVB, we assume that it can be utilized as an excellent photosensitizer for photodynamic/photothermal antimicrobial under sunlight.

### 3.3. Microbe imaging and photo-activated killing with TTVB

Prior to preparing a hybrid material bearing TTVB, the electrostatic interactions and photodynamic effects of TTVB on different pathogens were evaluated. Two Gram-positive bacterial strains (*Staphylococcus aureus* and multidrug-resistant *S. aureus* (MRSA)), two Gram-negative bacterial strains (*Escherichia coli* and multidrug-resistant (MDR) *E. coli*), two fungal strains (*Candida albicans* and *Saccharomyces cerevisiae*), and one viral strain (M13 bacteriophage) were chosen as model microbes. As shown in Fig. 1E, TTVB could stain all the tested bacterial and fungal strains benefiting from the strong electrostatic interaction between the positive charge of TTVB and the negative charge of cell envelopes. A higher concentration of TTVB was needed to stain *E. coli* and MDR *E. coli*, since Gram-negative bacteria are protected by an outer membrane containing lipopolysaccharide and other phospholipids to prevent the insertion of TTVB. The localization of TTVB in bacteria and fungi was determined in bacterial membrane and fungal mitochondria, respectively, as determined by using different organelle trackers (Figs. S6 and S7). By virtue of the broad-spectrum interaction to different microbes of TTVB, we then evaluated its antimicrobial performance upon irradiation with the simulated sunlight. As displayed in Fig. 1F and Fig. S8, without light irradiation, TTVB showed negligible toxicity to the bacteria and fungi. Whereas, upon light irradiation at an optical density of  $34 \text{ mW cm}^{-2}$ , the viability of TTVB-treated bacteria and fungi dropped rapidly, even almost complete bacterial inactivation within only 10 min irradiation. In the case of M13 bacteriophage, the situation is a little different because of the dark toxicity of TTVB towards

M13, nevertheless, TTVB also showed significant phototoxicity to M13 under the light. It is worth mentioning that the light-triggered microbicidal effect in solution is mainly originated from the ROS rather than the photothermal effect because of the insufficient photothermal conversion efficiency at a low concentration of TTVB (Fig. S5).

### 3.4. Preparation of TTVB-loaded nanofibrous membrane

Inspired by the broad-spectrum antimicrobial capability of TTVB on different pathogenic microbes, we then sought to fabricate a hybrid material promising for bioprotective equipment. To that end, the hybrid material should have a porous nanostructure to intercept pathogenic ultrafine particles. Thus, the electrospinning technique was adopted to prepare a TTVB-loaded nanofibrous membrane (TTVB@NM) with poly(vinylidene fluoride-co-hexafluoropropylene) (PVDF-HFP) as a polymer matrix. PVDF-HFP was chosen because of its electroactive property, which favors the electrostatic attraction of pathogenic particles onto the nanofibers [45,46]. The Fourier transform infrared (FTIR) spectra showed that upon doping of TTVB in nanofibrous membrane (NM), a new band around  $1585 \text{ cm}^{-1}$  corresponding to C=C stretching vibration appeared (Fig. S9). Furthermore, the thermal stability was evaluated with Differential Scanning Calorimetry (DSC) and Thermogravimetric Analysis (TGA). As a result, the melting points of NM and TTVB@NM are  $140.9 \text{ }^\circ\text{C}$  and  $138.0 \text{ }^\circ\text{C}$ , respectively, and the thermal decomposition temperatures are  $360.7 \text{ }^\circ\text{C}$  and  $433.2 \text{ }^\circ\text{C}$ . In addition, TTVB@NM has multi-layered nanofibrous morphology as shown in the scanning electron microscopy (SEM) images (Fig. 2B), and no significant microscopic architecture difference of the nanofibrous membrane (NM) was observed with and without dopants (Fig. S10). The average fiber diameter of NM without doping was  $479 \text{ nm}$  while that of TTVB@NM was a little larger showing an average at  $554 \text{ nm}$  (Fig. S11). The thickness of the nanofibrous membrane was measured to be around  $32 \mu\text{m}$

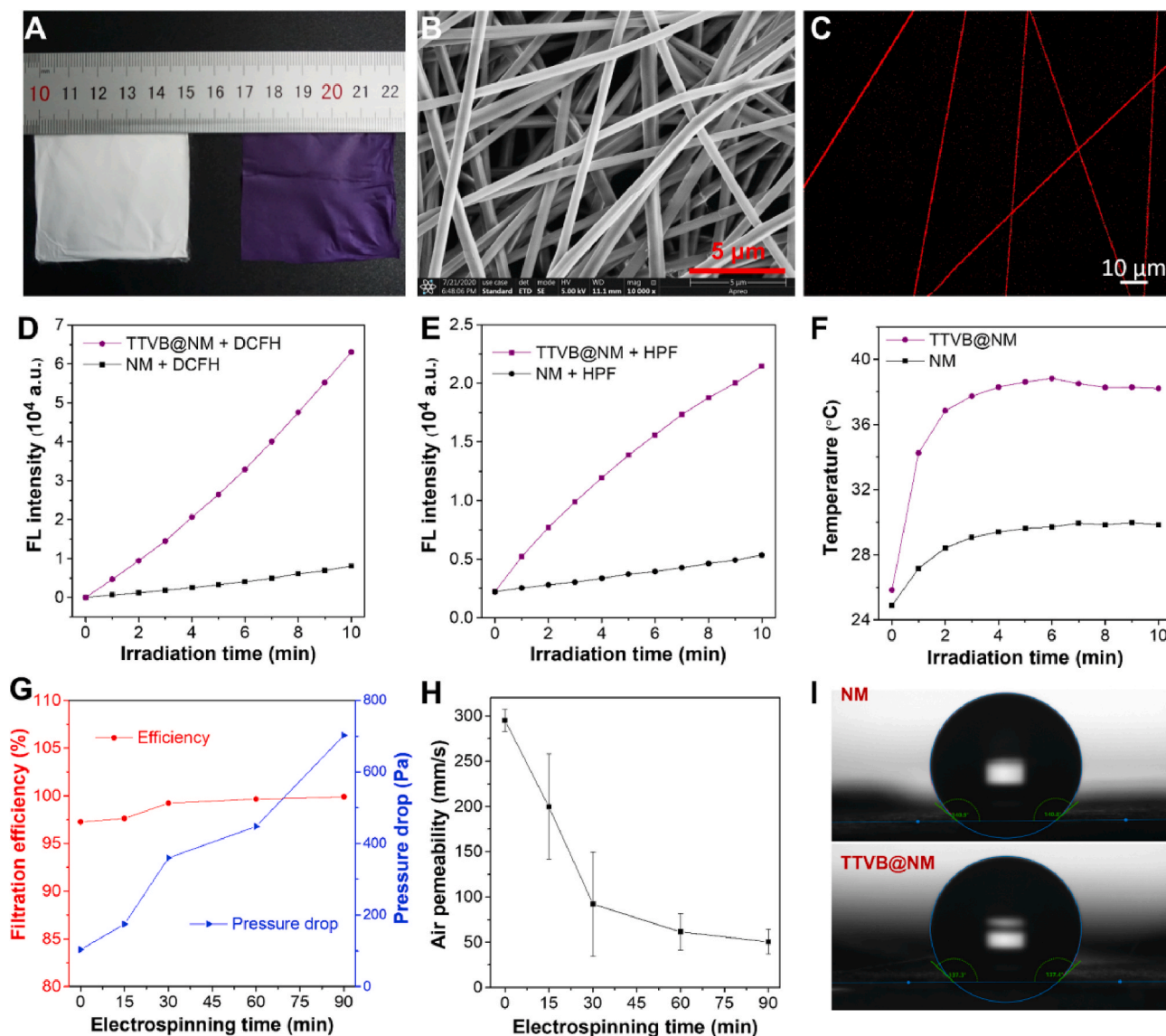


**Fig. 2.** (A) Photographs of NM and TTVB@NM. (B) SEM image and (C) CLSM image of TTVB@NM. (D) Total ROS generation of TTVB@NM under the irradiation of simulated sunlight ( $34 \text{ mW cm}^{-2}$ ). (E)  $\bullet\text{OH}$  radicals generation of TTVB@NM under the irradiation of simulated sunlight ( $34 \text{ mW cm}^{-2}$ ). (F) The photothermal conversion performance of NM and TTVB@NM under the irradiation of simulated sunlight ( $65 \text{ mW cm}^{-2}$ ). (G) Filtration efficiency and pressure drop of TTVB@NM as a function of electrospinning time. (H) Air permeability rate of TTVB@NM as a function of electrospinning time. (I) The water contact angles of NM and TTVB@NM at room temperature.

with an electrospinning time of 30 min (Fig. S12). The confocal laser scanning microscopy (CLSM) images revealed that TTVB was uniformly doped in all the fibers (Fig. 2C and Fig. S10). Importantly, the doping and electrospinning processes only had a slight effect on the light-harvesting ability of TTVB, and TTVB@NM still exhibited a broad absorption in the visible light range (400–700 nm) (Fig. S3).

### 3.5. ROS generation and photothermal property of TTVB@NM

Subsequently, the ROS generation ability of TTVB@NM was investigated by immersing the membrane in DCFH and HPF solution as indicators for total ROS and  $\bullet\text{OH}$ , respectively. It was observed that TTVB@NM generated massive ROS ( $\bullet\text{OH}$  in particular) as compared to NM without dopants, revealed by the increasing fluorescence intensity of DCFH and HPF with the elongation of irradiation time under simulated sunlight (Fig. 2D). The ROS generation capability was improved with the increasing of light intensity (Fig. S13). In addition, the photothermal conversion performance of TTVB@NM was estimated under the

irradiation of simulated sunlight at a power of  $65 \text{ mW cm}^{-2}$ . As a result, the temperature of NM and TTVB@NM increased from room temperature ( $25 \text{ }^\circ\text{C}$ ) to  $30 \text{ }^\circ\text{C}$  and  $38 \text{ }^\circ\text{C}$  within 5 min, respectively (Fig. 2F). When exposed to simulated sunlight at a power of  $100 \text{ mW cm}^{-2}$  that is almost the strongest intensity of natural sunlight in daily life, the temperature of TTVB@NM increased from room temperature ( $25 \text{ }^\circ\text{C}$ ) to  $43 \text{ }^\circ\text{C}$  (Fig. S14). Such temperature is much lower than the recently reported bioprotective materials ( $60\text{--}110 \text{ }^\circ\text{C}$ ) for microbial inactivation through only photothermal effect [47–49], nevertheless, it is sufficient to serve as an adjuvant role for the pathogen inhibition by accelerating the dehydration of pathogenic droplets and aerosols, without causing discomfort in contact with mouth and skin.

### 3.6. Filtration property and air-permeability of TTVB@NM

To meet the requirements of bioprotective equipment such as face mask, we studied the interception ability against ultrafine particles and the air-permeability of TTVB@NM prepared with different

electrospinning time. Since the nanofibrous membrane is too thin to peel off from the aluminum foil as a fully extended membrane if the electrospinning time is less than 1 h, TTVB@NM was collected on a piece of commercially provided melt-blowing fabric (MBF, thickness: 150  $\mu\text{m}$ ) to prepare samples for the following tests. The MBF itself without coating TTVB@NM was also tested and the results were plotted in Fig. 2G and H as the zero-time point. In the preliminary assessment, the filtration efficiency and pressure drop were measured against aerosols containing sodium chloride (NaCl) ultrafine particles with an average diameter of 260 nm at a constant airflow rate of 85 L  $\text{min}^{-1}$ . As depicted in Fig. 2G, by utilizing the electrospinning time of over 30 min, TTVB@NM coated

MBF exhibited higher filtration efficiency than the standard of the N99 face mask (filtration efficiency standard of N99: 99%). Meanwhile, TTVB@NM coated MBF showed increased pressure drops as a function of electrospinning time. When the electrospinning time is less than 30 min, the materials could satisfy the standard of the N99 face mask (pressure drop limit: 350 Pa at 85 L  $\text{min}^{-1}$ ). What's more, TTVB@NM coated MBF exhibited an acceptable air permeability ranging from 50 to 200  $\text{mm s}^{-1}$  under a constant pressure differential of 200 Pa (Fig. 2H). This value is comparable to even better than that of other antimicrobial wearable materials reported previously [50,51]. These results implied that TTVB@NM, at least in the terms of filtration efficiency and

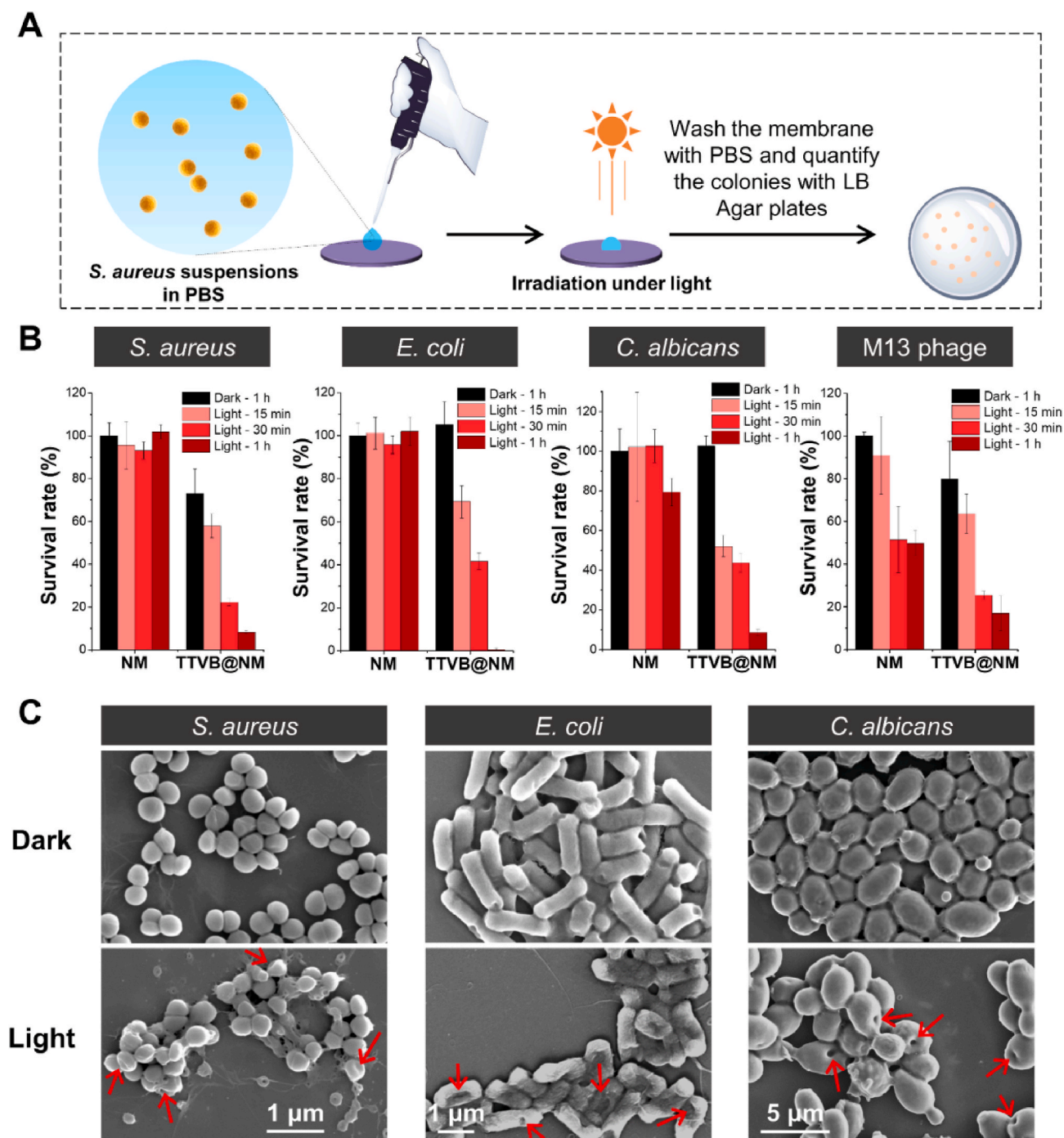


**Fig. 3.** (A) Schematic illustration of antimicrobial evaluation of TTVB@NM upon light irradiation against pathogenic droplet containing *S. aureus*. (B) Microbial survival rate in contact with NM or TTVB@NM in dark or under simulated sunlight ( $65 \text{ mW cm}^{-2}$ ). (C) Morphology of different microbes in contact with TTVB@NM in dark or under simulated sunlight ( $65 \text{ mW cm}^{-2}$ ) for 1 h.



air-permeability, was suitable for bioprotective equipment such as face masks and protective suits.

### 3.7. Antimicrobial activity by contact killing

Encouraged by the efficient ROS generation and particle interception ability of TTVB@NM, the microbial inactivation effect via contact inhibition was then examined against four model microbes: Gram-positive bacteria *S. aureus*, Gram-negative bacteria *E. coli*, fungi *C. albicans*, and M13 bacteriophage. The microbe suspensions were individually loaded onto NM or TTVB@NM and then kept in dark or exposed to simulated sunlight ( $65 \text{ mW cm}^{-2}$ ) for 15 min, 30 min, and 1 h, respectively (Fig. 3A). After that, the microbes were collected from the membranes using PBS buffer and the survival rates were determined by a typical plate colony-counting method. As shown in Fig. 3B and Fig. S15, in the case of bacteria and fungi, NM without dopants did not show evident microbicidal effect both under dark and simulated sunlight conditions, with microbial survival rates higher than 80%; TTVB@NM did not present antimicrobial performance in the dark, except for *S. aureus* against which around 30% antibacterial efficacy was observed; whereas, TTVB@NM exhibited significant microbicidal effects under the irradiation of simulated sunlight and less than 10% were survived upon irradiation for 1 h. In the case of M13 bacteriophage as the model virus (Fig. 3B and Fig. S15), the NM exhibited a moderate antiviral effect under the light with an inhibition efficacy of 50%; whereas, TTVB@NM showed more efficient antiviral performance under the light with an inhibition efficacy of more than 80%. Moreover, the field-emission SEM

was employed to observe the morphological changes of bacteria and fungi on the TTVB@NM membrane upon dark-incubation or exposure to simulated sunlight irradiation. As a result, clear morphology and surface integrity were observed for all the microbes kept in the dark. However, upon light illumination for 1 h on TTVB@NM, the microbes exhibited collapsed and shrunk surface, indicating the damaged cell membrane. In contrast, the microbes kept their morphology on NM both in dark and under light irradiation (Fig. S16). In addition, the antimicrobial activity of TTVB@NM was attributed to synergistic photodynamic and photo-thermal effects of TTVB. As shown in Fig. S17, when TTVB@NM was kept on ice to eliminate the photothermal effect, the antibacterial efficacy against *S. aureus* was weakened, and even more weakened upon further treatment with sodium ascorbate to partially eliminate ROS. It is worth mentioning that the water contact angles of NM ( $140.9^\circ$ ) and TTVB@NM ( $137.3^\circ$ ) have no big difference, indicating that the difference of antimicrobial efficacy is not a result from the difference of contact area (Fig. 2I). All these data solidly indicate the light-triggered decontamination ability of TTVB@NM toward a broad spectrum of microbes.

### 3.8. Antimicrobial activity against pathogenic aerosols

Apart from infectious droplets, airborne transmission caused by infectious aerosols is more likely a predominant transmission route for respiratory diseases because the small size (less than  $10 \mu\text{m}$ ) of aerosols enables a prolonged suspension time and long travel distance in the air [52]. Thereby, it is critical to investigate the interception and

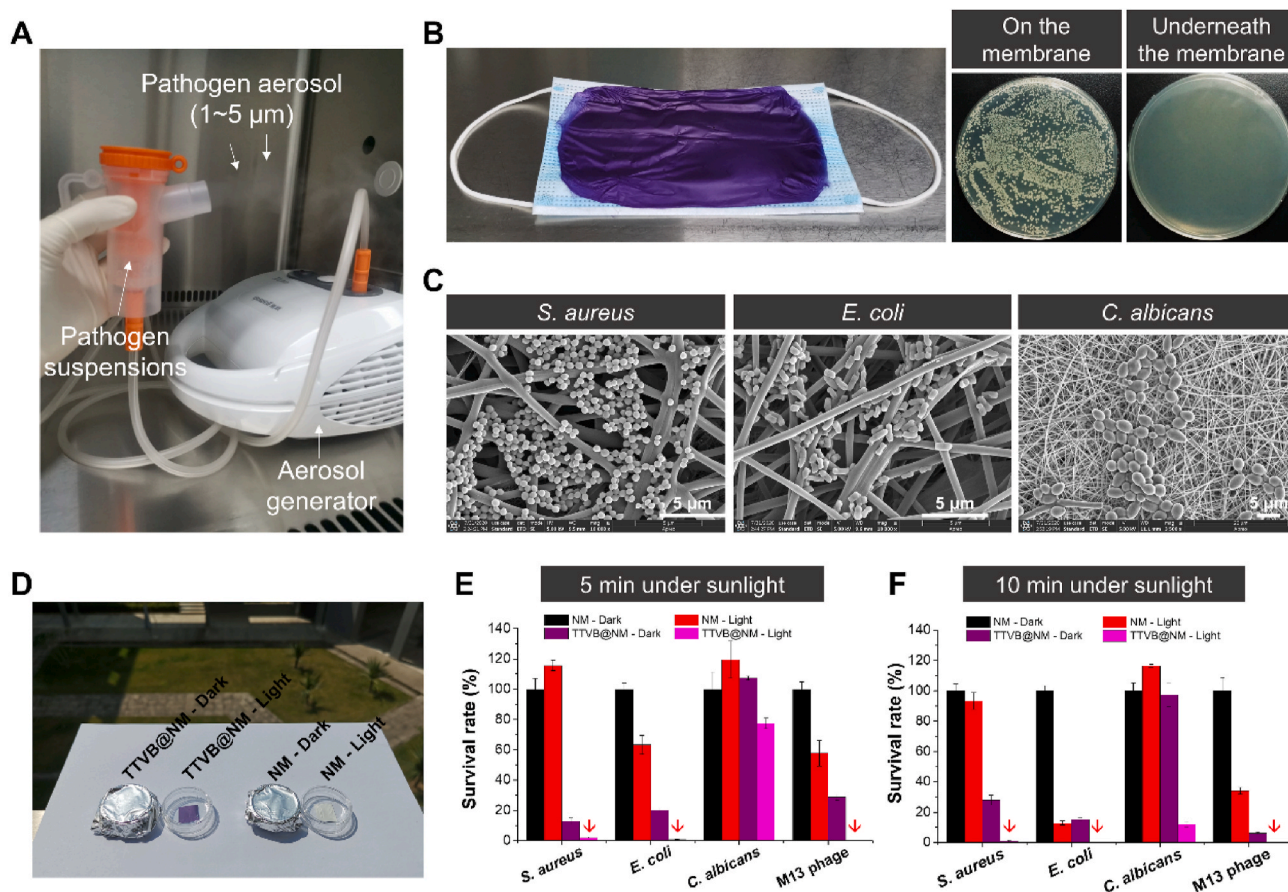


**Fig. 4.** (A) Pathogenic aerosols with a diameter of 1–5  $\mu\text{m}$  prepared using an aerosol generator. (B) TTVB@NM covered on a medical mask suffered from *E. coli* aerosols treatment and later analysis of live bacteria on and underneath the membrane using a plate-counting method. (C) SEM images of different microbes intercepted on the surface of TTVB@NM. (D) A picture of the antimicrobial experiment against aerosols containing mixed microbes under outdoor sunlight (sunlight intensity:  $83 \text{ mW cm}^{-2}$ , outdoor temperature:  $26^\circ\text{C}$ ) and survival rates of different microbes after (E) 5 min or (F) 10 min sunbathing. (Red arrows: antimicrobial efficacy is around 100%). (For interpretation of the references to color in this figure legend, the reader is referred to the Web version of this article.)

disinfection effects of TTVB@NM against pathogenic aerosols under simulated sunlight. Pathogenic aerosols with a diameter of 1–5  $\mu\text{m}$  were produced by an aerosol generator to mimic the aerosols generated by human sneezing or coughing (Fig. 4A). *E. coli*-containing aerosols were firstly prepared as model infectious aerosols to study the interception ability of TTVB@NM mimicking the medical mask (Fig. 4B). After spraying *E. coli* aerosols to TTVB@NM for 10 s at an airflow rate of 0.2  $\text{mL min}^{-1}$ , the population of living *E. coli* on and underneath the membrane was analyzed using a plate-counting method. It was found that a bunch of bacteria was collected from the upper surface of the membrane, while no bacteria were detected on the medical mask which is underneath the membrane (Fig. 4B). Same results were also obtained with aerosols containing *S. aureus*, *C. albicans*, and M13 phage (Fig. S18). Subsequently, the interception of those pathogens on the upper surface was confirmed by SEM observations (Fig. 4C). Furthermore, the disinfection effect of TTVB@NM to pathogenic aerosols was evaluated against four different pathogenic strains, including Gram-positive bacteria *S. aureus*, Gram-negative bacteria *E. coli*, fungi *C. albicans*, and M13 bacteriophage. NM and TTVB@NM were sprayed with different aerosols containing individual pathogen for 20 s at a flow rate of 0.2  $\text{mL min}^{-1}$  and then kept in the dark or under simulated sunlight (65  $\text{mW cm}^{-2}$ ) for 5 or 10 min. After that, the membranes were washed with PBS and the number of live pathogens was determined on solid plates. As shown in Fig. S19, in the case of control experiments performed on NM, a similar number of bacteria, fungi, and bacteriophages were collected from the membrane either in the dark or under the light, whereas, the pathogen viability was remarkably reduced on TTVB@NM once exposed to simulated sunlight for only 5 or 10 min. SEM images of the microbes on TTVB@NM after light irradiation were also taken. However, due to the antimicrobial ability of TTVB@NM under light, most microbes were destructed and could be easily flushed away during the preparation of the SEM samples and only a few microbes were observed (Fig. S20).

Inspired by the above results, we then wondered whether the microbes could be inactivated on TTVB@NM under natural sunlight. To better simulate the situations in real life, we prepared aerosols containing mixed microbes. NM and TTVB@NM loaded with pathogenic aerosols were transferred to outdoor (sunlight intensity: 83  $\text{mW cm}^{-2}$ , outdoor temperature: 26  $^{\circ}\text{C}$ ) and irradiated under sunlight for 5 min or 10 min (Fig. 4D). After that, the pathogens were collected from the membranes and the numbers of survival pathogens were quantified using different solid plates: LB-agar plates for quantification of *E. coli* and *S. aureus*, YPD-agar plates for *C. albicans*, and LB/IPTG/X-gal plates for M13 bacteriophage (Fig. S21). As shown in Fig. 4E, NM did not have an antimicrobial effect except for a moderate inhibition to *E. coli* (37%) and M13 (~42%) under sunlight. TTVB@NM had a plain killing effect in the dark, which can be attributed to the positive charge of TTVB, as demonstrated in the literature that the surface-immobilized quaternary-ammonium-compounds can serve as a contact-killing coating.<sup>8</sup> Importantly, TTVB@NM exhibited a significant pathogen inactivation effect and even eliminated more than 99% of all *S. aureus*, *E. coli*, and M13 after only 5 min's sunbathing. In the case of *C. albicans*, 90% of inhibition efficiency was achieved by extending the irradiation time to 10 min, which was a much shorter time than the literature-reported materials for the potential bioprotective applications [10,14,53]. All these results indicated that TTVB@NM could serve as a sunlight-triggered decontamination surface that can not only intercept but also kill microbes in both droplets and aerosols.

### 3.9. Washability and photostability of TTVB@NM

The leaching of photosensitizer from the antimicrobial membrane in aqueous solution is unfavorable for their long-term use in practical applications. To evaluate the washability of TTVB@NM, we immersed the membrane with a size of 1  $\text{cm}^2$  in 1 mL of water for 48 h and monitored the leaching of TTVB by recording the UV-vis absorption spectra of the

aqueous solution at different time points (Fig. S22). In addition, RB@NM was prepared by electrospinning technique with a commercial photosensitizer Rose Bengal as dopants and the washability of RB@NM was tested for comparison. As a result, there is no leaching of TTVB from TTVB@NM in water. On the other hand, RB@NM is less tolerant to the washing process due to the water solubility of RB and more than 80% of RB leached out after immersing in water for 48 h.

The photostability of photosensitizer-doped nanofibrous membrane is essential for the photodynamic antimicrobial ability. Therefore, we evaluated the photostability of TTVB@NM under daylight. As shown in Fig. S23, after 7 days' exposure, the antibacterial efficacy of TTVB@NM against *S. aureus* still maintained, indicating that the service life is more than one week.

## 4. Conclusion

In summary, we have demonstrated the preparation of a new nanofibrous membrane (TTVB@NM) as a sunlight-triggered photodynamic/photothermal antimicrobial surface against a broad spectrum of microbes including bacteria, fungi, and viruses. TTVB@NM was facilely fabricated by the electrospinning technique with an AIEgen TTVB as the dopant and electroactive PVDF-HFP as the polymer matrix. The multi-layered porous structure of TTVB@NM favored the interception of pathogenic droplets and aerosols. TTVB@NM exhibited a wide absorption in the visible light range, a high ROS-generation efficiency, and moderate photothermal conversion efficiency, endowing it with extraordinary antimicrobial performance against pathogenic aerosols under sunlight irradiation for only 5–10 min. This study thus provides useful insights into constructing reusable and ease-to-sterilize bioprotective equipment.

### Author contributions

M. L. and D. W. conceived the idea and designed the experiments. H. W. synthesized and characterized TTVB. H. L. helped M. L. to prepare and characterize NM and TTVB@NM. M. L. performed all the antibacterial experiments and discussed with Y. L. and Z.-C. Y. All the authors discussed the results and commented on the manuscript. D. W. and B. Z. T. supervised the overall research. M. L. and D. W. wrote the manuscript.

### Declaration of competing interest

The authors declare that they have no known competing financial interests or personal relationships that could have appeared to influence the work reported in this paper.

### Acknowledgments

This work was partially supported by the China Postdoctoral Science Foundation Grant (2020M672813, 2020M672797), the Natural Science Foundation for Distinguished Young Scholars of Guangdong Province (2020B1515020011), the National Natural Science Foundation of China (21801169, 21803039), and the Science and Technology Foundation of Shenzhen City (JCYJ20190808153415062, RCYX20200714114525101). The authors acknowledge Prof. Xiaolin Huang in Nanchang University for providing M13 bacteriophage and its host bacteria ER2738. The authors also acknowledge the Instrumental Analysis Center of Shenzhen University.

### Appendix A. Supplementary data

Supplementary data to this article can be found online at <https://doi.org/10.1016/j.biomaterials.2021.121007>.

## References

- [1] X. Liu, S. Zhang, COVID-19: face masks and human-to-human transmission. *Influenza other respi, Viruses* 14 (2020) 472–473.
- [2] P. Laskar, M.M. Yallapu, S.C. Chauhan, "Tomorrow never dies": recent advances in diagnosis, treatment, and prevention modalities against coronavirus (COVID-19) amid controversies, *Diseases* 8 (2020) 30.
- [3] M.H. Chua, W. Cheng, S.S. Goh, J. Kong, B. Li, J.Y.C. Lim, L. Mao, S. Wang, K. Xue, L. Yang, E. Ye, K. Zhang, W.C.D. Cheong, B.H. Tan, Z.B. Li, B.H. Tan, X.J. Loh, Face masks in the new COVID-19 normal: materials, testing, and perspectives, *Research* 2020 (2020) 7286735.
- [4] M.E. Tomas, S. Kundrapu, P. Thota, V.C. Sunkesula, J.L. Cadnum, T.S. Mana, A. Jencson, M. O'Donnell, T.F. Zabarsky, M.T. Hecker, A.J. Ray, B.M. Wilson, C. J. Donskey, Contamination of health care personnel during removal of personal protective equipment, *JAMA Intern. Med.* 175 (2015) 1904–1910.
- [5] D. Ji, L. Fan, X. Li, S. Ramakrishna, Addressing the worldwide shortages of face masks, *BMC Mater* 2 (2020) 9.
- [6] B. Simoncic, B. Tomic, Structures of novel antimicrobial agents for textiles - a review, *Textil. Res. J.* 80 (2010) 1721–1737.
- [7] L. Rizzello, P.P. Poma, Nanosilver-based antibacterial drugs and devices: mechanisms, methodological drawbacks, and guidelines, *Chem. Soc. Rev.* 43 (2014) 1501–1518.
- [8] Z. Li, H. Bai, S. Jia, H. Yuan, L.-H. Gao, H. Liang, Design of functional polymer nanomaterials for antimicrobial therapy and combatting resistance, *Mater. Chem. Front.* 5 (2021) 1236–1252.
- [9] L.A.T.W. Asri, M. Crismaru, S. Roest, Y. Chen, O. Ivashenko, P. Rudolf, J.C. Tiller, H.C. van der Mei, T.J.A. Loontjens, H.J. Busscher, A shape-adaptive, antibacterial-coating of immobilized quaternary-ammonium compounds tethered on hyperbranched polyurea and its mechanism of action, *Adv. Funct. Mater.* 24 (2014) 346–355.
- [10] Q.C. Wang, X.J. Yu, M. Libera, Reducing bacterial colonization of 3-D nanofiber cell scaffolds by hierarchical assembly of microgels and an antimicrobial peptide, *Adv. Healthc. Mater.* 2 (2013) 687–691.
- [11] F. Vatanever, W.C.M.A. de Melo, P. Avci, D. Vecchio, M. Sadasivam, A. Gupta, R. Chandran, M. Karimi, N.A. Parizotto, R. Yin, G.P. Tegos, M.R. Hamblin, Antimicrobial strategies centered around reactive oxygen species - bactericidal antibiotics, photodynamic therapy, and beyond, *FEMS Microbiol. Rev.* 37 (2013) 955–989.
- [12] T. Maisch, J. Baier, B. Franz, M. Maier, M. Landthaler, R.M. Szeimies, W. Baumler, The role of singlet oxygen and oxygen concentration in photodynamic inactivation of bacteria, *P. Natl. Acad. Sci. USA* 104 (2007) 7223–7228.
- [13] P. Tang, Z. Zhang, A.Y. El-Moghazy, N. Wisuthiphaet, N. Nitin, G. Sun, Daylight-induced antibacterial and antiviral cotton cloth for offensive personal protection, *ACS Appl. Mater. Interfaces* 12 (2020) 49442–49451.
- [14] Y. Si, Z. Zhang, W. Wu, Q. Fu, K. Huang, N. Nitin, B. Ding, G. Sun, Daylight-driven rechargeable antibacterial and antiviral nanofibrous membranes for bioprotective applications, *Sci. Adv.* 4 (2018) eaar5931.
- [15] D. Yang, X. Lv, L. Xue, N. Yang, Y. Hu, L. Weng, N. Fu, L. Wang, X. Dong, A lipase-responsive antifungal nanoplatfor for synergistic photodynamic/photothermal/pharmaco-therapy of azole-resistant *Candida albicans* infections, *Chem. Commun.* 55 (2019) 15145–15148.
- [16] H. Zhang, Y. Liang, H. Zhao, R. Qi, Z. Chen, H. Yuan, H. Liang, L. Wang, Dual-Mode antibacterial conjugated polymer nanoparticles for photothermal and photodynamic therapy, *Macromol. Biosci.* 20 (2020) 1900301.
- [17] J. Kim, H. Lee, J.-Y. Lee, K.-H. Park, W. Kim, J.H. Lee, H.-J. Kang, S.W. Hong, H.-J. Park, S. Lee, J.-H. Lee, H.-D. Park, J.Y. Kim, Y.W. Jeong, J. Lee, Photosensitized production of singlet oxygen via C<sub>60</sub> fullerene covalently attached to functionalized silica-coated stainless-steel mesh: remote bacterial and viral inactivation, *Appl. Catal. B Environ.* 270 (2020) 118862.
- [18] Y. Lhotáková, L. Plíštil, A. Morávková, P. Kubát, K. Lang, J. Forstová, J. Mosinger, Virucidal nanofiber textiles based on photosensitized production of singlet oxygen, *PLoS One* 7 (2012), e49226.
- [19] B.L. Carpenter, F. Scholle, H. Sadeghifar, A.J. Francis, J. Boltersdorf, W.W. Weare, D.S. Argyropoulos, P.A. Maggard, R.A. Ghiladi, Synthesis, characterization, and antimicrobial efficacy of photomicrobicidal cellulose paper, *Biomacromolecules* 16 (2015) 2482–2492.
- [20] D.R. Alvarado, D.S. Argyropoulos, F. Scholle, B.S.T. Peddinti, R.A. Ghiladi, A facile strategy for photoactive nanocellulose-based antimicrobial materials, *Green Chem.* 21 (2019) 3424–3435.
- [21] S. Marklund, Spectrophotometric study of spontaneous disproportionation of superoxide anion radical and sensitive direct assay for superoxide dismutase, *J. Biol. Chem.* 251 (1976) 7504–7507.
- [22] M. Garcia-Diaz, Y.-Y. Huang, M.R. Hamblin, Use of fluorescent probes for ROS to tease apart type I and type II photochemical pathways in photodynamic therapy, *Methods* 109 (2016) 158–166.
- [23] H. Sies, Strategies of antioxidant defense, *Eur. J. Biochem.* 215 (1993) 213–219.
- [24] B. Yang, Y. Chen, J. Shi, Reactive oxygen species (ROS)-Based nanomedicine, *Chem. Rev.* 119 (2019) 4881–4985.
- [25] M. Cho, H. Chung, W. Choi, J. Yoon, Different inactivation behaviors of MS-2 phage and *Escherichia coli* in TiO<sub>2</sub> photocatalytic disinfection, *Appl. Environ. Microbiol.* 71 (2005) 270–275.
- [26] S.M. Imani, L. Ladouceur, T. Marshall, R. MacLachlan, L. Soleymani, T.F. Didar, Antimicrobial nanomaterials and coatings: current mechanisms and future perspectives to control the spread of viruses including SARS-CoV-2, *ACS Nano* 14 (2020) 12341–12369.
- [27] E. Horvath, L. Rossi, C. Mercier, C. Lehmann, A. Sienkiewicz, L. Forro, Photocatalytic nanowires-based air filter: towards reusable protective masks, *Adv. Funct. Mater.* 30 (2020) 2004615.
- [28] J.S. Ni, T.L. Min, Y.X. Li, M.L. Zha, P.F. Zhang, C.L. Ho, K. Li, Planar AIEgens with enhanced solid-state luminescence and ROS generation for multidrug-resistant bacteria treatment, *Angew. Chem. Int. Ed.* 59 (2020) 10179–10185.
- [29] X. Li, S. Lee, J. Yoon, Supramolecular photosensitizers rejuvenate photodynamic therapy, *Chem. Soc. Rev.* 47 (2018) 1174–1188.
- [30] M.M. Kang, C.C. Zhou, S.M. Wu, B.R. Yu, Z.J. Zhang, N. Song, M.M.S. Lee, W.H. Xu, F.J. Xu, D. Wang, L. Wang, B.Z. Tang, Evaluation of structure-function relationships of aggregation-induced emission luminogens for simultaneous dual applications of specific discrimination and efficient photodynamic killing of gram-positive bacteria, *J. Am. Chem. Soc.* 141 (2019) 16781–16789.
- [31] M.M.S. Lee, D.Y. Yan, J.H.C. Chau, H. Park, C.C.H. Ma, R.T.K. Kwok, J.W.Y. Lam, D. Wang, B.Z. Tang, Highly efficient phototheranostics of macrophage-engulfed gram-positive bacteria using a NIR luminogen with aggregation-induced emission characteristics, *Biomaterials* 261 (2020) 120340.
- [32] H. Chen, S.L. Li, M. Wu, Kenry, Z.M. Huang, C.S. Lee, B. Liu, Membrane-anchoring photosensitizer with aggregation-induced emission characteristics for combating multidrug-resistant bacteria, *Angew. Chem. Int. Ed.* 59 (2020) 632–636.
- [33] X.W. He, Y.J. Yang, Y.C. Guo, S.G. Lu, Y. Du, J.J. Li, X.P. Zhang, N.L.C. Leung, Z. Zhao, G.L. Niu, S.S. Yang, Z. Weng, R.T.K. Kwok, J.W.Y. Lam, G.M. Xie, B. Z. Tang, Phage-guided targeting, discriminative imaging, and synergistic killing of bacteria by AIE bioconjugates, *J. Am. Chem. Soc.* 142 (2020) 3959–3969.
- [34] H. Bai, W. He, J.H.C. Chau, Z. Zheng, R.T.K. Kwok, J.W.Y. Lam, B.Z. Tang, AIEgens for microbial detection and antimicrobial therapy, *Biomaterials* (2020), 120598.
- [35] S.D. Xu, Y.K. Duan, B. Liu, Precise molecular design for high-performance luminogens with aggregation-induced emission, *Adv. Mater.* 32 (2020) 1603530.
- [36] W.H. Xu, M.M.S. Lee, Z.H. Zhang, H.H.Y. Sung, I.D. Williams, R.T.K. Kwok, J.W. Y. Lam, D. Wang, B.Z. Tang, Facile synthesis of AIEgens with wide color tunability for cellular imaging and therapy, *Chem. Sci.* 10 (2019) 3494–3501.
- [37] D. Wang, M.M.S. Lee, W.H. Xu, G.G. Shan, X.Y. Zheng, R.T.K. Kwok, J.W.Y. Lam, X. L. Hu, B.Z. Tang, Boosting non-radiative decay to do useful work: development of a multi-modality theranostic system from an AIEgen, *Angew. Chem. Int. Ed.* 58 (2019) 5628–5632.
- [38] Z.J. Zhang, W.H. Xu, M.M. Kang, H.F. Wen, H. Guo, P.F. Zhang, L. Xi, K. Li, L. Wang, D. Wang, B. Tang, An all-round athlete on the track of phototheranostics: subtly regulating the balance between radiative and nonradiative decays for multimodal imaging-guided synergistic therapy, *Adv. Mater.* 32 (2020) 2003210.
- [39] Y.X. Zhang, H. Fu, D.E. Liu, J.X. An, H. Gao, Construction of biocompatible bovine serum albumin nanoparticles composed of nano graphene oxide and AIEgen for dual-mode phototherapy bacteriostatic and bacterial tracking, *J. Nanobiotechnol.* 17 (2019) 104.
- [40] D. Wang, M.M.S. Lee, W.H. Xu, R.T.K. Kwok, J.W.Y. Lam, B.Z. Tang, Theranostics based on AIEgens, *Theranostics* 8 (2018) 4925–4956.
- [41] D. Wang, M.M.S. Lee, G.G. Shan, R.T.K. Kwok, J.W.Y. Lam, H.F. Su, Y.C. Cai, B. Z. Tang, Highly efficient photosensitizers with far-red/near-infrared aggregation-induced emission for in vitro and in vivo cancer theranostics, *Adv. Mater.* 30 (2018) 1802105.
- [42] D. Wang, H.F. Su, R.T.K. Kwok, X.L. Hu, H. Zou, Q.X. Luo, M.M.S. Lee, W.H. Xu, J. W.Y. Lam, B. Tang, Rational design of a water-soluble NIR AIEgen, and its application in ultrafast wash-free cellular imaging and photodynamic cancer cell ablation, *Chem. Sci.* 9 (2018) 3685–3693.
- [43] L. Bourre, S. Thibaut, A. Briffaud, N. Rousset, S. Eleouet, Y. Lajat, T. Patrice, Indirect detection of photosensitizer ex vivo, *J. Photochem. Photobiol., B* 67 (2002) 23–31.
- [44] D. Yang, Y. Tu, X. Wang, C. Cao, Y. Hu, J. Shao, L. Weng, X. Mou, X. Dong, A photo-triggered antifungal nanoplatfor with efflux pump and heat shock protein reversal activity for enhanced chemo-photothermal synergistic therapy, *Biomater. Sci.* 9 (2021) 3293–3299.
- [45] S. Roy, P. Thakur, N.A. Hoque, B. Bagchi, S. Das, Enhanced electroactive  $\beta$ -phase nucleation and dielectric properties of PVDF-HFP thin films influenced by montmorillonite and Ni(OH)<sub>2</sub> nanoparticle modified montmorillonite, *RSC Adv.* 6 (2016) 21881–21894.
- [46] A. Al-Saygh, D. Ponnamma, M.A. AlMaadeed, P.P. Vijayan, A. Karim, M.K. Hassan, Flexible pressure sensor based on PVDF nanocomposites containing reduced graphene oxide- titania hybrid nanolayers, *Polymers* 9 (2017) 33.
- [47] H. Zhong, Z.R. Zhu, P. You, J. Lin, C.F. Cheung, V.L. Lu, F. Yan, C.Y. Chan, G.J. Li, Plasmonic and superhydrophobic self-decontaminating N95 respirators, *ACS Nano* 14 (2020) 8846–8854.
- [48] L. Huang, S. Xu, Z. Wang, K. Xue, J. Su, Y. Song, S. Chen, C. Zhu, B.Z. Tang, R. Ye, Self-reporting and photothermally enhanced rapid bacterial killing on a laser-induced graphene mask, *ACS Nano* 14 (2020) 12045–12053.
- [49] Z.Z. Lin, Z. Wang, X. Zhang, D.F. Diao, Superhydrophobic, photo-sterilize, and reusable mask based on graphene nanosheet-embedded carbon (GNEC) film, *Nano Res* 14 (2020) 1110–1115.
- [50] H. Li, W. Zhang, Q. Ding, X. Jin, Q. Ke, Z. Li, D. Wang, C. Huang, Facile strategy for fabrication of flexible, breathable, and washable piezoelectric sensors via welding of nanofibers with multiwalled carbon nanotubes (MWCNTs), *ACS Appl. Mater. Interfaces* 11 (2019) 38023–38030.
- [51] X. Peng, K. Dong, C. Ye, Y. Jiang, S. Zhai, R. Cheng, D. Liu, X. Gao, J. Wang, Z. L. Wang, A breathable, biodegradable, antibacterial, and self-powered electronic

- skin based on all-nanofiber triboelectric nanogenerators, *Sci. Adv.* 6 (2020), eaba9624.
- [52] J. Gralton, E. Tovey, M.L. McLaws, W.D. Rawlinson, The role of particle size in aerosolised pathogen transmission: a review, *J. Infect.* 62 (2011) 1–13.
- [53] J.Y. Zhuo, G. Sun, Antimicrobial functions on cellulose materials introduced by anthraquinone vat dyes, *ACS Appl. Mater. Interfaces* 5 (2013) 10830–10835.